Ammonia recovery in bipolar membrane electrodialysis via pH control through electric current pulse modulation

Kaniadakis, Iosif; van Lier, Jules B.; Spanjers, Henri

DOI
10.1016/j.watres.2025.124185

Publication date
2025

Document Version
Final published version

Published in
Water Research

Water Research 286 (2025) 124185

Contents lists available at ScienceDirect

Water Research

journal homepage: www.elsevier.com/locate/watres

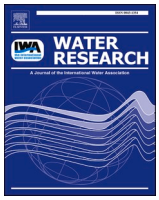

Ammonia recovery in bipolar membrane electrodialysis via pH control through electric current pulse modulation

Iosif Kaniadakis *, Jules B. van Lier, Henri Spanjers

Faculty of Civil Engineering and Geosciences, Delft University of Technology, Stevinweg 1, Delft 2628 CN, the Netherlands

ARTICLE INFO

Keywords:
Electrodialysis
pH control
Ammonia stripping
Bipolar membrane
Vacuum membrane stripping

ABSTRACT

Despite growing scientific interest in the past decade, bipolar membrane electrodialysis has seen limited advancement in controlled operation of water dissociation via the bipolar membrane (BPM). For nutrient recovery applications, such as ammonia (NH_3) extraction from anaerobic digestion reject water, implementing in-situ pH control in the base solution could enhance energy efficiency. By controlling the electric current, pH is regulated through OH^- generation from the bipolar membrane (BPM). Once the targeted pH is reached, the electric current is applied in pulses and pauses with the purpose to sustain and to not overpass the pH setpoint. A selective electrodialysis reversal (SEDR) combined with a two-compartment bipolar membrane electrodialysis (BPMC) and vacuum membrane stripping (VMS) enabled the recovery and conversion of ammonium ions (NH_4^+) into volatile ammonia (NH_3). Operating the BPMC with the developed pH control method lowered energy consumption ($E_{NH_4^+}$) and improved current efficiency for NH_4^+ removal compared to constant current (CC) operation. Under pH control, the BPMC maintained the target pH throughout the whole operation, with an $E_{NH_4^+}$ between 12.5 and 35.3 MJ·kgN^{-1}, compared to 12.1 and 78.6 MJ·kgN^{-1} under CC. The current efficiency was maintained across setpoints with pH control, ranging between 25 % and 29 %. With CC, the current efficiency declined from 27 % to 12 % at higher current densities. Furthermore, pH control applying a pulsed electric current reduced the occurrence of scaling by minimising the transport of divalent cations across the cation exchange membrane and CO_2 formation in the acid compartment. Similar removal efficiencies were attained, applying pH controlled operation and CC; however, both methods performed a declining removal efficiency during 30 h operation. The developed pH control method can provide distinct improvement in scale-up applications, where energy reduction by preventing excessive water dissociation by the BPM is of interest. In addition, external caustic dosing can be substituted by pH control with a BPMC layout of the stack, reducing the residual impurities of the chemical dosing.

Abbreviations

SEDR	Selective Electrodialysis Reversal
BPMC	Bipolar Membrane Electrodialysis utilizing Cation exchange membranes
VMS	Vacuum Membrane Stripping
σ	Electrical Conductivity
ED	Electrodialysis
BPMED	Bipolar Membrane Electrodialysis
CC	Constant Current
I_d	Current Density
CEM	Cation-Exchange Membrane
MCEM	Monovalent Cation-Exchange Membrane
AEM	Anio-Exchange Membrane
BPM	Bipolar Membrane
$E_{NH_4^+}$	Energy consumption for NH_4^+ removal
$\eta_{\%}$	Current efficiency for NH_4^+ transport
AD	Anaerobic Digestion
$RE(t,\%)$	Removal Efficiency of NH_4^+
CP	Concentration Polarisation
PEF	Pulsed Electric Field
VFAs	Volatile Fatty Acids
C	total Coulombs
PID	Proportional Integral Derivative
CIP	Cleaning In Place

* Corresponding author.
E-mail address: i.kaniadakis@tudelft.nl (I. Kaniadakis).

https://doi.org/10.1016/j.watres.2025.124185
Received 1 May 2025; Received in revised form 25 June 2025; Accepted 7 July 2025
Available online 8 July 2025

1. Introduction

In contemporary studies over the past decade, the potential of electrochemical recovery of NH_3 from NH_4^+-rich streams has been explored with high interest (Deng et al., 2021). Bipolar membrane electrodialysis (BPMED) is notable for its ability to produce acid and base solutions without external addition of chemicals. By incorporating ion-exchange membranes, BPMED separates cations and anions from the feed solution. The cation-exchange membrane (CEM) allows the transport of cations, while the anion-exchange membrane (AEM) allows the transport of anions. Furthermore, the incorporation of the bipolar membrane (BPM) facilitates the production of protons (H^+/H_3O^+) and hydroxyl ions (OH^-). In a conventional three-compartment BPMED setup, an acid solution is formed in the acid by concentrating anions and H_3O^+, and a base solution is created by concentrating cations and OH^-.

1.1. Targeting required pH values with BPMED

In previous studies, BPMED was utilised to recover valuable resources and nutrients at a specific required pH. In the study conducted by Shi et al. (2018), BPMED successfully recovered volatile fatty acids (VFAs) and ammonia (NH_3) in the acid and base solutions, respectively. It was mentioned that the basicity in the base must exceed the pKb of NH_3 to provide a product suitable for NH_3 stripping while the acidity was of ideal conditions to recover the VFAs in their acidic form. With a similar objective, conventional electrodialysis (ED) was utilized to recover VFAs, however, an external chemical dosing for pH adjustment was incorporated, indicating the necessity of controlled pH in ED/BPMED (Kotoka et al., 2024). Apparently, pH-control in BPMED is considered of high importance, especially in processes where gaseous products are aimed for, such as NH_3 or CO_2. While a basic pH higher than the pKb of NH_3 is required for effective recovery, for CO_2 the acid compartment pH must be lower than the pKa of CO_2 (Sharifian et al., 2022). BPMED has been successfully used as an alternative to thermal regeneration for CO_2 capture from flue gas, with pH being regulated by the dosing of external caustics and acids (Jiang et al., 2017; Valluri and Kawatra, 2021). According to recent studies, BPMED can successfully recover NH_3 from various NH_4^+-rich solutions in the base (Kaniadakis et al., 2024; Li et al., 2021, 2016; van Linden et al., 2020b). In addition, the concentrated NH_3(aq) in the base solution of BPMED can be further extracted by vacuum membrane stripping (VMS) via a membrane contactor (EL-Bourawi et al., 2007; Saabas and Lee, 2022; van Linden et al., 2022b). Notably, the efficiency of the NH_3 stripping process is closely linked to the high basicity of the base solution and the volatilization of NH_3. To maintain the stripping efficiency of the NH_3-air stripping process, other researchers applied external addition of NaOH in the NH_3-solution (Guillen-Burrieza et al., 2023; Limoli et al., 2016; Palakodeti et al., 2022). According to Guillen-Burrieza et al. (2023), external addition of NaOH for NH_3 stripping via a membrane distillation unit from the centrate side-stream accounted for 39 % of the overall operational costs. Moreover, the amount of NaOH required for the conversion of NH_4^+ into NH_3 depends on the concentration of NH_4^+ and the buffer capacity of the base solution. In cases where the treated feed is reject water from anaerobic digestion (AD) (or digestate effluent), the main buffering agent is the bicarbonate ion HCO_3^- (Guillen-Burrieza et al., 2023; van Linden et al., 2020b). Because the bicarbonate concentration in AD reject water varies, the amount of required NaOH may vary as well (Quist-Jensen et al., 2018). As an alternative, the costs associated with acid and alkali dosing can be reduced by their in-situ production with BPMED, while the subsequent NH_3 recovery can be achieved by incorporating VMS. The energy consumption for NH_3 recovery is expected to be in the range between 22.7 and 42.8 $MJ \cdot gN^{-1}$ for BPMED (Ferrari et al., 2022; Guo et al., 2023; van Linden et al., 2020b) and 7 $MJ \cdot gN^{-1}$ for VMS (EL-Bourawi et al., 2007; van Linden et al., 2022a), which is energy-wise compatible with the Haber-Bosch process for NH_3 production, using natural gas as H_2 source (Capdevila-Cortada, 2019; Kyriakou et al., 2020) .

1.2. pH control in BPMED

pH control in ED and BPMED is critical for maintaining optimal conditions for both energy efficiency and product quality. In the literature, pH regulation has been achieved either through the external addition of chemicals or via a programmable process. Specifically, external pH control in BPMED has been implemented through the external addition of acid or base (Readi et al., 2013; Arslan et al., 2017; Wu et al., 2025). Alternatively, programmable methods have been explored to modulate pH without chemical dosing. Chen et al. (2012) demonstrated that pH gradients in ED can be generated by adjusting the electrode water splitting rate. Nomura et al., (1988) presented a tunable pH control strategy for acetic acid production via ethylene oxidation in an electrodialytic cell. More recently, Rodrigues et al. (2023) employed a proportional-integral-derivative (PID) controller to regulate the feed flow rate in BPMED, mitigating excessive acidification caused by free H_3O^+ generation at the BPM. However, programmable control of the water dissociation of a BPM by intermittent applied current for NH_3 recovery in BPMED has not been reported in literature.

1.3. Concentration gradient as driving force for NH_4^+ transport by diffusion

The driving force for cation transport based on concentration gradient and ionic electric mobility in membrane systems has been well described in previous studies (Kamcev et al., 2018; Paul, 2004; Wijmans and Baker, 1995). According to the Nernst-Planck equation (Eq. (1)), the concentration gradient leads to transport by diffusion, while the electric field causes electro-migration (Tanaka, 2007). Eq. (2) expresses the ionic electric mobility per ion diffusion coefficient.

$$J_i = D_i \frac{dC_i}{dx} + D_i \frac{Fz_iC_i}{RT} \frac{du}{dx} \quad (1)$$

$$\mu_i = \frac{D_i}{RT} \quad (2)$$

Where, for ion i, J_i is the ionic flux ($mol \cdot m^{-2} \cdot s^{-1}$), D_i is the diffusion coefficient of each ion ($10^{-9} \cdot m^2 \cdot s^{-1}$) (Table 1), C_i is ionic concentration ($mol \cdot m^{-3}$), x is the spatial coordinate, where in this case, the membrane cross-section (m), z_i is the valence, F is the Faraday constant ($C \cdot mol^{-1}$), R is the universal gas constant ($J \cdot K^{-1} \cdot mol^{-1}$), T is the temperature of fluid (K), u is the applied electric potential (V), and μ is the electric ionic electric mobility in water ($10^{-8} \cdot m^2 \cdot (V \cdot s)^{-1}$) . It is assumed that upon introducing a high concentration gradient in the ED, a greater transport of NH_4^+ will be facilitated, due to its higher propensity for diffusion through the CEM compared to other cations, as outlined in Table 1. At low pH, the competition between NH_4^+ and H_3O^+ ions increases (Mutahi et al., 2024). Since NH_4^+ is present in much higher concentrations than the divalent cations it becomes the dominant charge carrier. According to Table 1, the diffusion coefficient of NH_4^+ ($1.98 \cdot 10^{-9}$ $m^2 \cdot s^{-1}$) compared to Ca^{2+} ($0.79 \cdot 10^{-9}$ $m^2 \cdot s^{-1}$) and Mg^{2+} ($0.71\ 0 \cdot 10^{-9}$ $m^2 \cdot s^{-1}$) is almost two times higher meaning that, in theory, in ED less divalent cations diffuse than NH_4^+.

1.4. Pulsed applied current for preferential transport of monovalent over divalent cations in electrodialysis

In ED, the faster diffusion and migration rates of monovalent cations compared to divalent cations can be strategically leveraged by applying short intervals of electric current, such as with pulsed electric fields (PEF). Andreeva (2018) demonstrated that low-frequency PEF reduces the transport of divalent ions like Ca^{2+} and Mg^{2+} relative to monovalent cations, allowing ionic concentrations at the boundary layer to revert to bulk phase levels during pause. Therefore, intermittently pulsed applied

Table 1
Transport properties of common cations in reject water. The tendency of NH_4^+ ion to diffuse faster than the competitive divalent cations is expected, given its higher diffusion coefficient (D_i), greater electric mobility, higher molarity in solution and smaller hydrated radius. Competitive transport of H_3O^+ could occur due to its much higher diffusion coefficient compared to NH_4^+.

Ion	Hydrated radius(nm)	*Diffusion coefficient (10^{-9} $m^2 \cdot s^{-1}$)	^Electric mobility in water 10^{-8} $\cdot m^2 \cdot (V \cdot s)^{-1}$	Molarity in solution, *this study* (mM)
H^+ as H_3O^+	0.280	5.31	36.3	pH dependent
K^+	0.331	1.96	7.6	14.9
NH_4^+	0.331	1.98	7.6	44.42
Na^+	0.358	1.33	5	3.9
Ca^{2+}	0.412	0.79	6.2	1.5
Mg^{2+}	0.428	0.70	5.5	9.9

* Retrieved from PHREEQC database.
^ Retrieved from Aspen Plus V12 database.

current can potentially improve the current efficiency for monovalent cations like NH_4^+over divalent like Ca^{2+} (Sosa-Fernandez et al., 2020). When comparing NH_4^+ and Na^+, lower current densities (I_d) favoured the transport of the former, indicating that reduced electric current can enhance the movement of cations with higher diffusion coefficients and smaller ionic radii (Ozkul et al., 2023; Rodrigues et al., 2021, 2020). Moreover, monovalent cations exhibit higher diffusion coefficients, facilitating their preferential transport in multi-cationic solutions over divalent cations (Ozkul et al., 2024). In studies of Rodrigues et al. (2021, 2023) intermittent applied current to promote Donnan diffusion of NH_4^+ significantly reduced scaling formation and improved the energy consumption for NH_4^+ removal. Therefore diffusion could be partially employed as an additional driving force for preferential transport of NH_4^+ to reduce the competition against Ca^{2+} and Mg^{2+} and delay scaling formation.

1.5. The problem with concentrating and converting NH_4^+ to NH_3 in BPMED

BPMED serves two primary functions: water dissociation and ion concentration, both driven by an applied electric current (Strathmann, 2010). Optimizing NH_4^+ transport and the conversion to NH_3 in BPMED minimizes unnecessary water dissociation (Rathod et al., 2024). Mohammadi et al. (2021) shows that improved distribution of applied electric current by reducing the operational time improves NH_3 formation. This suggests that shorter, more intense cycles may be more efficient than longer, lower-intensity operational duration. Applying excessive electric current in BPMC configuration can reduce the NH_4^+ current efficiency and NH_3 conversion resulting in difficulty to sustain high basicity (Mutahi et al., 2024; Saabas and Lee, 2022). In BPMED, a high applied electric current or potential leads to a high production of H_3O^+ and OH^- in the acid and base solution, respectively (Mani, 1991). However, control of electric current in BPMC to control the pH in the acid and base solution has not been yet reported in literature.

1.6. Research objective: implementing pulsed current to regulate OH^- generation and favour NH_4^+ transport

Previous research has demonstrated the feasibility of in-situ pH and electric current control in ED and BPMED configurations. In this study, we combined selective electrodialysis reversal (SEDR) with BPMC and VMS with pH control in the base solution to reduce excessive water dissociation. The primary goal is to reduce the energy consumption and improve the current efficiency for NH_4^+ transport by limiting excess OH^- generation in proportion to the available NH_4^+ mass in the base. We also show that pH control via the BPMC can facilitate NH_3 stripping without requiring external chemical additives. The pH is controlled via the electric current pulse modulation, which is applied as irregular pulses and pauses. The secondary goal to further tackle the challenge of complex water matrices, like AD reject water, includes the pulse-pause application of electric current to improve the current efficiency on NH_4^+ transport in the presence of other competing cations. Additionally, we investigated the impact of controlled pH applications on total mass transport, comparing outcomes between pH control and constant current operation.

2. Materials and methods

2.1. pH control on BPMC

The significance of controlled BPMC operation is particularly evident in practical, on-site applications, where in-situ control of the electric current can be utilized to regulate key variables such as pH, stack resistance, and scaling formation. In a BPMC+VMS system for NH_3 recovery, the pH of the base solution can be regulated through the power supply unit (PSU), since OH^- generation from the BPM is driven by the applied electric current.

In this study, pH control of the base solution in BPMC was implemented by modulating the power supply to operate with pulses and pauses of applied current density (I_d). The aim is to keep the basicity at a targeted pH, described as setpoint. Le Chatelier's principle dictates that in an aqueous solution, when NH_4^+ reacts with OH^- to form NH_3, an equilibrium between NH_3 and H_3O^+ (as per Eq. (3)) is established. Upon removal of NH_3 from the solution, the equilibrium shifts to the right, resulting in an increase in the concentration of H_3O^+ ions, consequently leading to more acidic pH. Thus, a reduction in NH_3 concentration indicates the stripping of NH_3 and the need for additional electric current to transport more NH_4^+ into the base. Additionally, the generation of OH^- is activated to maintain the target pH.

$$NH_4^+ + H_2O \rightleftharpoons NH_3 + H_3O^+ \quad (3)$$

With NH_4^+ being present in higher concentrations alongside the CEM, the driving force of diffusion will enable NH_4^+ transport during the pause phase when no current is applied. Therefore, by introducing a pause phase in BPMC operation, NH_4^+ transport via diffusive migration is maximised, while electro-migration is minimised as shown in Fig. 1. Concomitantly, unnecessary water dissociation and the transport of divalent cations is minimised, which will reduce possible scaling if saturation in the base is prevented.

2.2. Reject water

The AD reject water was sampled from the municipal sewage treatment plant of Horstermeer, The Netherlands with the following composition of mean values with min-max deviation: Cl^- 950 ± 250 $mg \cdot L^{-1}$, PO_4^{3-} 136 ± 14 $mg \cdot L^{-1}$, SO_4^{2-} 15 ± 5 $mg \cdot L^{-1}$, Na^+ 96.5 ± 5.5 $mg \cdot L^{-1}$, K^+ 466 ± 116 $mg \cdot L^{-1}$, Mg^{2+} 305 ± 65 $mg \cdot L^{-1}$, NH_4^+ 700 ± 170 $mg \cdot L^{-1}$, Ca^{2+} 72.5 ± 14.5 $mg \cdot L^{-1}$, HCO_3^- 3378 ± 539 $mg \cdot L^{-1}$, pH 7.8, TOC 114.5 ± 20.5 $mg \cdot L^{-1}$, and TSS 192 $mg \cdot L^{-1}$

2.3. Setup

Both SEDR and BPMC cells were manufactured and supplied by RedStack B.V. (Sneek, The Netherlands) with an active surface area of 10

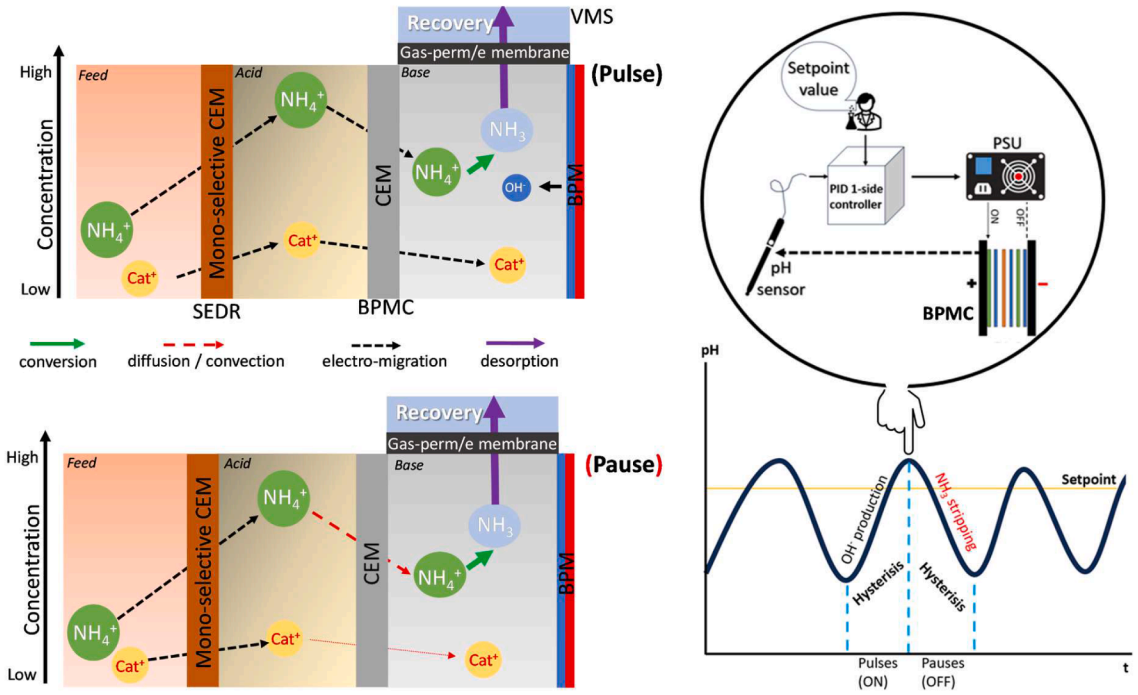

Fig. 1. The operational principles of pH-controlled NH_3 recovery with SEDR+BPMC+VMS. Initially the SEDR continuously transports NH_4^+ and other cations (Cat^+) by electro-migration. During the pulse phase in the BPMC, the BPM produces OH^- from the dissociation of H_2O. The produced OH^- and the transported NH_4^+ by electro-migration are combined to form NH_3 in the base solution. During the pause phase, the NH_4^+ from the acid was transported into the base by diffusion only due to the concentration gradient, while the remaining NH_3 in the base was removed from the solution by desorption in the VMS. This mechanism results in less basic pH of the base, which triggers the pH controller to switch on the power supply for a new pulse phase.

× 10 cm of Pt/Ir coating with TiO_2-stretched metal.

2.4. Selective electrodialysis reversal (SEDR)

The ED module operated as SEDR, consisted of ten pairs of AEMs (FAS-PET-130) supplied by Fumatech, Germany, and monovalent CEMs (CXP-S) supplied by ASTOM, Japan. The diluate and the concentrate compartments consisted of 0.27 mm thickness wire mesh spacers made of silicon/polyethylene sulfone and two CEM end-membranes of F-10,150-PTFE. To regulate the applied current in the SEDR, a digital time relay from Crouzet, France, operating within 20–240 V AC/DC, was interfaced with the power supply, providing a timed cycle of 75s: 5 s (forward: reverse).

2.5. Bipolar membrane electrodialysis (BPMC)

The BPMC contained ten cell pairs each consisting of one BPM of FBM-BPM and one CEM of FKB-PK-130 supplied by Fumatech, Germany.

2.6. Vacuum membrane stripping module (VMS)

A custom-designed VMS module, developed by TRIMEM, The Netherlands, was employed in this study. The module featured expanded polytetrafluoroethylene (ePTFE) membranes and consisted of four membrane channels measuring 500 mm in length, 600 mm in width, and 2 mm in spacer thickness. Additionally, five vacuum channels were incorporated, each measuring 500 mm in length, 600 mm in width, and featuring spacer thicknesses of 3 mm 0·7 mm and 2 mm · 4 mm. The total membrane surface area was 2 m^2.

2.7. Vacuum pressure and temperature control

A vacuum membrane pump type N 820.3FT.18 from KNF, (Neuberg, Germany) was used to apply vacuum pressure. The vacuum pressure was set at −0.8 bar and was controlled based on an inline pressure sensor (ifm electronic, Essen, Germany). The temperature of the base solution was controlled at 35 °C by the inline heater Profi RVS 1 kW connected to a thermostat. A Grundfos pump connected to a float sensor was installed for the regulation of the base solution volume for overnight operations.

2.8. Sensors and electrical configuration

The electric current for the SEDR cell was supplied by a Delta Elektronika power supply series SM800, providing a voltage range of 00.00–18.37 V and a current range of 00.00–50.00 A. Similarly, the BPMC unit received the electric current from the Delta Elektronika power supply series SM1500, which has a voltage range of 000.00–120.00 V and a current range of 00.00–13.00 A. The circulation of solutions through the modules was controlled by calibrated Seaflo diaphragm pumps from Xiamen Doofar Outdoor Co., Ltd., China, while the diluate was fed into the SEDR via a calibrated Grundfos pump Bjerrinbro, Denmark. Solution pH was monitored using Endress and Hauser calibrated pH probes, specifically Memosens CPS11E in PVC in-lined armatures, linked to an 8-channel CM448 Liquiline transmitter. Electrical conductivities (EC) were measured with QC205X electrodes coupled with a P915–85 controller from QiS-Prosence BV, Oosterhout, The Netherlands. pH and electrical conductivity (σ) data were logged using a MultiCon CMC-99 data logger provided by SIMEX, Gdansk, Poland. Additionally, all the water samples were analysed via Ion Chromatography using the Metrohm Compact IC Flex 930, with 883 cation system for cations (Na^+, NH_4^+,K^+, Mg^{2+}, Ca^{2+}) and 818 anion system for anions (Cl^-, SO_4^{2-}, PO_4^{3-}).

2.9. Operational conditions

The process scheme is shown in Fig. 2 where reject water was fed continuously from a 1 m^3 storage tank into the SEDR+BPMC+VMS configuration. To avoid reaching depletion of the acid solution and

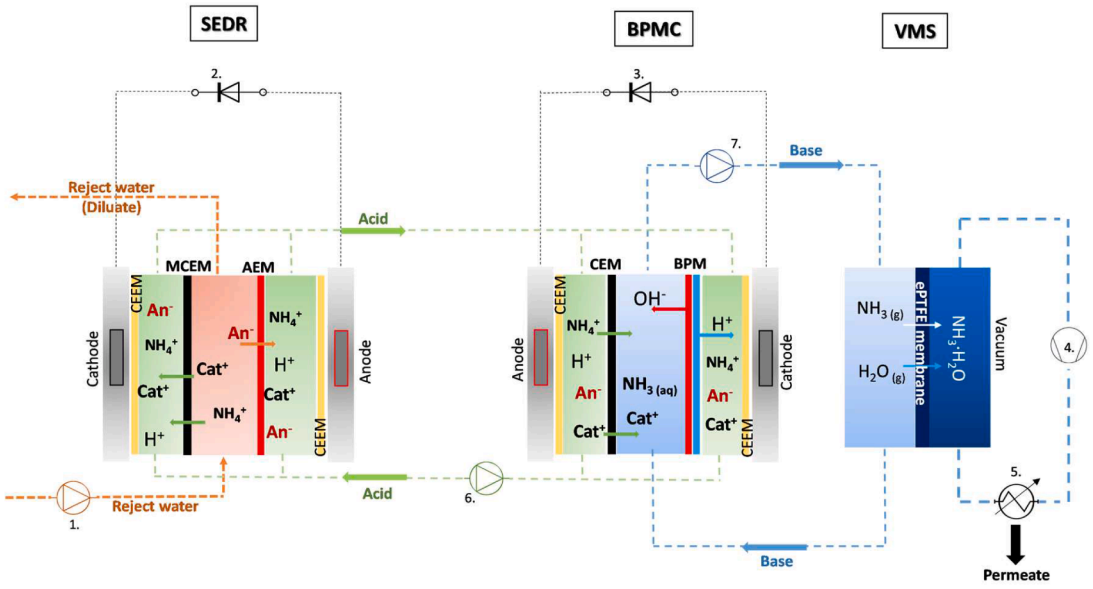

Fig. 2. The NH_3 recovery process from reject water using SEDR, BPMC, and VMS modules. Initially, the SEDR established the concentration gradient by transporting ions from the feed to the acid compartment, with the MCEM promoting the transport of monovalent cations. The produced diluate came as the desalinated feed. Simultaneously, the BPMC, through water dissociation facilitated by the BPM, produced both acid and base solutions, while transporting cations from the acid to the base. In the base solution, transported NH_4^+ was converted to NH_3. Once the target pH was reached, the VMS was activated. This enabled the desorption of volatile NH_3 through the ePTFE membrane under vacuum, where it was collected as the final product. In addition, the process scheme includes the feeding pump (1), the power supplies for SEDR and BPMC (2,3), the vacuum pump (4), the cooling collection-bottle (5) and the recirculation pumps for the acid (6) and base (7) solutions.

ensure consistency of the SEDR, the feeding rate and the applied I_d in SEDR were adjusted per experiment according to the load ratio concept (Kaniadakis et al., 2024; Rodríguez Arredondo et al., 2017). The load ratio of 0.8 was applied in SEDR and was adjusted based on the varying NH_4^+ concentration in the feed. During non-control experiments, the BPMC was operated at conditions of constant current (CC) with I_d of 40, 75, 85 and 120 $A{\cdot}m^{-2}$ to reach the setpoint in the base of 9.2, 9.5, 10 and 10.5, respectively. For the experiments with pH control in the base, the selected pH setpoints were 9.2, 9.5, and 10 at 75 $A{\cdot}m^{-2}$ and pH 10.5 at 85 $A{\cdot}m^{-2}$. All the experiments were performed for a duration of at least 30 h in duplicates and in total 870 L of reject water were treated.

2.10. Performance indicators

The energy consumption for SEDR and BPMC as $J{\cdot}gN^{-1}$ and converted to $MJ{\cdot}kgN^{-1}$:

$$E_{NH_4^+} = \frac{\sum_{t=0}^{t}(U_t{\cdot}I_t{\cdot}\Delta t)}{m_{NH_4^+,}\ \Delta t} \quad (4)$$

where $U_{\Delta t}$ = average electric potential (in V) over a time interval Δt (s) between two sampling points, $I_{\Delta t}$ = average applied current during the time interval (in A), $m_{NH_4^+}$ = the difference in mass (g) of NH_4^+ between a sampling time interval Δt.

The current efficiency for the present cations in BPMC was determined as a fraction of the total charge:

$$\eta_{\%i} = \frac{z{\cdot}F{\cdot}\Delta M_i}{N{\cdot}\sum_{t=0}^{t}(I_d{\cdot}\Delta t)}\cdot 100\% \quad (5)$$

Where $\eta_{\%i}$ is the current efficiency for cation i, z is the ion valance, F the Faraday constant, ΔM the molarity difference across the referred time interval, N the number of pairs, I_d the applied current density ($A{\cdot}m^{-2}$) and Δt the time interval (s).

The NH_4^+ removal efficiency ($RE(t,\%)$) by the BPMC is expressed as:

$$RE(t,\%). = \left(\frac{m_{\ NH_4^+,\ ED,t} - m_{NH_4^+,\ acid,t}}{m_{NH_4^+,\ ED,t}}\right)\cdot 100\% \quad (6)$$

Where $RE(t,\%)$ is the NH_4^+ removal efficiency over a sampling time interval, $m_{\ NH_4^+,\ ED,t}$ is the mass of NH_4^+ transported by the SEDR during the time interval and $m_{\ NH_4^+,\ acid,t}$ the final mass of NH_4^+ remained in the acid solution.

3. Results and discussion

3.1. The pH profile in base and acid solution during pH control

Faraday's law relates the amount of produced H_3O^+ and OH^- by the BPM with the intensity of the applied current density (Blommaert et al., 2021; Sharifian et al., 2021). Consequently, in a BPMC stack aiming for a high basic pH in the base results to a corresponding high acidic pH in the acid. Fig. 3 shows the pH in the base and acid over 30 h in total of pH-controlled operation in the BPMC. In the base, the targeted pH setpoints of 9.2, 9.5, 10 and 10.5 were achieved. During the initial time the BPMC operated constantly until the pH setpoint was reached and the pH control operation was activated. Once a steady state was achieved, the controlled basicity of the base solution resulted in a corresponding oscillating acidification of the acid solution. Changes in oscillations were also observed during the activation of the water-supply pump/float sensor communication in the base when the system was left unsupervised during the night. Furthermore, when the pH in the base was adjusted to a value higher than the pKb of NH_3, a corresponding drop in the pH of the acid occurred, falling below the pKa of CO_2. However, the production of CO_2 in this process was disadvantageous since it can potentially diffuse through the CEM, contributing to the formation of scaling (Kaniadakis et al., 2024). The fluctuations of the pH in the base solution resulted due to the pulses and pauses of applied electric current and the pressure and temperature control in the VMS. The production of OH^- ions occurred during pulses led to pH increase. In addition, the conversion of $NH_4^+$to NH_3 and the simultaneous removal via vacuum stripping led to pH decrease. In the acid, during the pause phase, the ongoing delivery of HCO_3^- ions by the SEDR, coupled with the diffusion of CO_2 through the CEM, resulted in a rise in pH. Conversely, during the pulse phase, the generation of $H_3O^+$by the BPM induced acidification of the solution, resulting in a decrease of pH. At a pH setpoint of 9.2, the

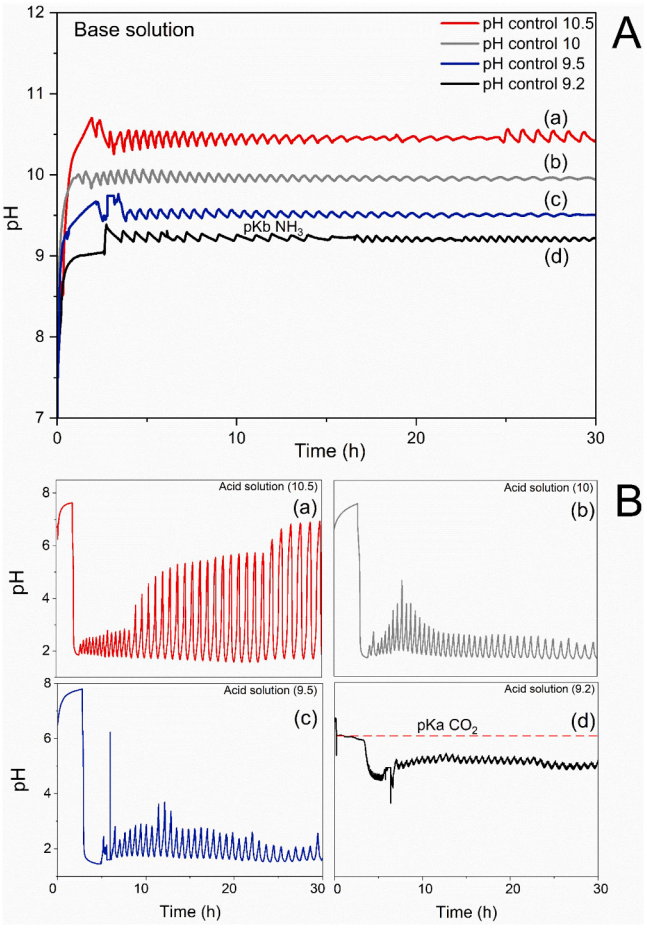

Fig. 3. Fig. 3A shows the four experiments, applying pH control in the base at pH 9.2, 9.5, 10, and 10.5. Fig. 3B shows the corresponding effect on H_3O^+production in the acid solution, indicated with the letters a, b, c, and d. The pH oscillations in the base solution were caused by two main factors: the production of OH^- by the BPM during the pulses, and the removal of NH_3 during the pauses. Likewise, the oscillations in the acid solution resulted from production of $H_3O^+$by the BPM during the pulses and their rapid depletion during pauses, due to simultaneous reaction with the transported HCO_3^- from the SEDR into the acid.

production of H_3O^+ and OH^- ions was theoretically lower, whereas at a setpoint of 10.5, the production was the highest.

3.2. Effect of BPMC with pH control on current efficiency ($\eta_{\%}$)

Regarding NH_4^+, the $\eta_{\%}$ was <30 % for both methods, similar to previous studies on BPMC configuration, where averages between 20 % and 25 % have been reported (Ferrari et al., 2022; Rodrigues et al., 2023). Fig. 4 shows the $\eta_{\%}$ for the operations of CC (Fig. 4(a)) and pH control (Fig. 4(b)). The $\eta_{\%}$ for NH_4^+ was lower than previously reported studies on ED and BPMED configurations (Ippersiel et al., 2012; Mondor et al., 2008; van Linden et al., 2019; Ward et al., 2018). The excess of H_3O^+ in the acid could be the reason for these transport losses as H_3O^+may compete with NH_4^+ (Mutahi et al. 2024). Although in the study of (Rodrigues et al., 2023), the H_3O^+ competition was not dominant due to less acidic pH, in this study the pH of the acid was below the pH of 3 for every experiment on CC. The theoretical amount of transported protons (presented as H_3O^+) were calculated based on the H_3O^+ balance described by Faraday's law and the pH drop in the base for both operational conditions.

Fig. 4(a) shows that the $\eta_{\%}$ of NH_4^+ diminished, while the $\eta_{\%}$ for H_3O^+ transport became dominant, when the experiments progressed under higher I_d. These results align with the observation that higher I_d produce more H_3O^+. Furthermore, the back diffusion of NH_3 to the acid and its re-transport as ionised NH_4^+ could also negatively affect the $\eta_{\%}$ (van Linden et al., 2020b). During CC operation, the targeted pH value in the base did not stabilise. The diffusion of H_3O^+ in a BPMC configuration might explain the pH reduction in the base as it was shown and extensively described by (Saabas and Lee, 2022). Furthermore, the lower $\eta_{\%}$ of NH_4^+, especially under conditions with high basicity, could be attributed to increased precipitation of multivalent cations on the CEM. Although the $\eta_{\%}$ for Ca^{2+} and Mg^{2+} were negligible compared to that of H_3O^+ and NH_4^+, the presence of precipitation was still evident.

In Fig. 4(b), the $\eta_{\%}$ of H_3O^+ with pH control was dominant at high pH setpoints, due to more acidic pH in the acid, increasing the driving force for H_3O^+ diffusion and electro-migration into the base. Nevertheless, pH control provided more stable $\eta_{\%}$ than CC for each pH setpoint, i.e., 9.2, 9.5, 10 and 10.5, which could be explained by the gradient-driven diffusion of NH_4^+ during pauses. During pH control at the setpoint of 9.2, the H_3O^+ competition was the lowest, due to the increased pH in the acid. However, when the setpoint was increased, the $\eta_{\%}$ of H_3O^+ increased simultaneously, indicating more free H_3O^+ were transported or diffused from the acid to the base at these higher setpoints. Increased H_3O^+concentrations resulted from increased water dissociation that generates OH^- and H_3O^+ in a 1:1 ratio (Pärnamäe et al., 2021). Therefore, a higher basicity of the base should ideally correspond to a higher

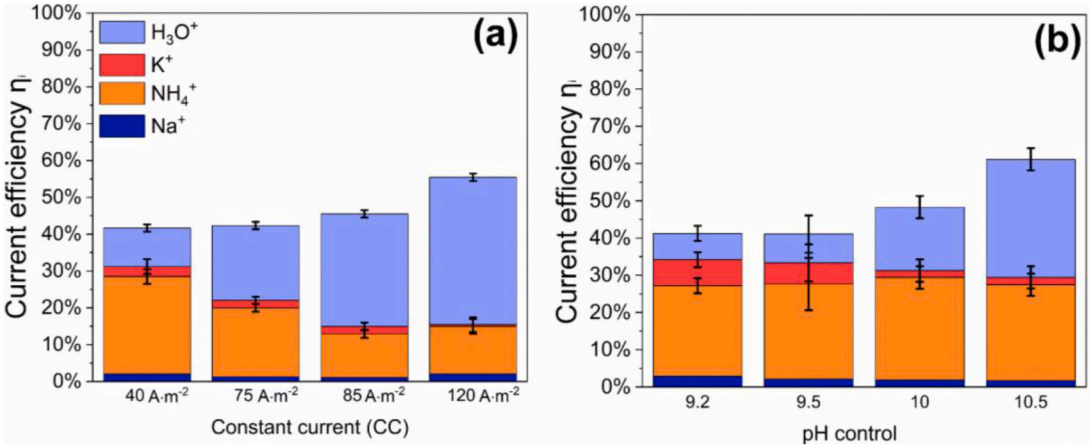

Fig. 4. The current efficiency $\eta_{\%}$ of cations through the CEM of the BPMC for the whole operational time. (a) Constant current operation at applied current densities 40, 75, 85, and 120 $A \cdot m^{-2}$. (b) pH control operation at pH setpoints 9.2, 9.5, 10 and 10.5.

acidity in the acid. At a pH of 10.5, the $\eta_{\%}$ of H_3O^+ was highest, driving the majority of the current.

The $\eta_{\%}$ for K^+ was higher with pH control compared to the CC method, with the difference being most pronounced at pH levels of 9.2 and 9.5. Under these conditions, the $\eta_{\%}$ for K^+ reached approximately 8 % with pH control, compared to only 2 % with the CC method. The application of either a pulsed or constant electric current had a different effect on the cation transport across the CEM. Monovalent cations more effectively utilized the electric field due to their higher electric mobility under a pulsed electric current, which provided an advantage over divalent cations such as Ca^{2+} and Mg^{2+} and indicated reduced concentration polarization (CP) (Honarparvar et al., 2023; Sosa-Fernandez et al., 2020).

The diffusion and transport priority of monovalent cations in electrodialysis is strongly positive influenced by their concentration in the solution (Yang et al., 2023). Additionally, a higher volume ratio from the feed to the concentrate solution in electrodialysis amplifies differences in diffusion behaviour among monovalent cations (Sun et al., 2022). In this study NH_4^+ exhibited the highest concentration among the cations, and the employed acid-to-base volume ratio of 1:3 further favoured its selective transport, resulting in a higher $\eta_{\%}$ compared to Mg^{2+} and Ca^{2+}. Quantitatively, it was estimated that the pulse phase accounted for approximately 71–96 % of the total NH_4^+ flux, while the pause phase contributed to 13–21 %. Regarding the transport of divalent cations, the pause phase contributed to only 4–11 % of the total transport, indicating the advantage of monovalent cations during pause (Fig. S1).

In summary, operations without pH control, thus under CC conditions, led to an average reduced $\eta_{\%}$ for NH_4^+ with a range between 12 % and 28 %. Conversely, pH control ensured that the $\eta_{\%}$ of NH_4^+ remained between 25 % and 29 % by average, particularly for higher pH setpoints.

Fig. 5 shows the total applied coulombs by the BPMC for the CC method (Fig. 5(a)) and the pH control method (Fig. 5(b)). The total time during which the PSU was active differed between the two methods. With the CC operation, the BPMC had a predictable total operational time. However, with pH control, the PSU was only active for part of the total operational period. Fig. 5(b) shows that the cumulative applied coulombs by the BPMC increased proportionally with the duration of pulse operation. This indicates that pH control allows for targeted application of electric current to maintain the desired pH level, therefore utilising less total coulombs.

3.3. Improved $E_{NH_4^+}$ with pH control in BPMC

Fig. 6 shows that during the experimental runs conducted with pH control, the $E_{NH_4^+}$ was consistently lower compared to CC. Over the course of 30 h of operation, the $E_{NH_4^+}$ increased due to the cumulative resistance across the CEM. With regards to the CC method in Fig. 6(a), scaling was the main constituent factor of the raised resistance. Although the MCEM effectively reduced the transport of divalent cations to the acid, a small amount of Ca^{2+} and Mg^{2+} was still able to migrate with time and eventually oversaturate in the base. In Fig. 6(b), the experiments with pH control showed stable $E_{NH_4^+}$ with marginal increase over time. In ED systems, the $E_{NH_4^+}$ is proportional to the transported NH_4^+ mass, time duration, and total power input (voltage and applied electric current). All the experiments with pH control demonstrated lower average voltage levels and a shorter PSU activation time compared to CC operation. Consequently, $E_{NH_4^+}$ was lower with pH control, particularly due to the lower formed resistance on the CEM surface. As described by Andreeva et al. (2018), an applied electric current of low pulsing frequency results in a relaxation and regeneration of the concentration profile that occurs on the boundary layer of the CEM, mitigating CP phenomena.

Despite the negligible amount of Ca^{2+} and Mg^{2+}, scaling was still evident and crucially affected the process. In combination with the diffusion of CO_2 into the base, the formation of $CaCO_3$ and $MgCO_3$ took place. Notably, the generation of CO_2 in the acid was distinctly enhanced when the pH in the acid dropped below the pKa of CO_2. As shown by Tran et al. (2013), higher concentrations of CO_3^{2-}, Ca^{2+} and Mg^{2+} at high basicity can result in severe scaling formation in the base. Furthermore, due to high concentrations of cations in the acid, the phenomenon of CP negatively affected the $E_{NH_4^+}$, similarly to the reduced $\eta_{\%}$ at higher I_d. With pH control, a more efficient distribution of charge or $I_d$was achieved.

Throughout the 30-hour operation, no cleaning in place (CIP) was carried out in the base compartment, which might have contributed to a lower $E_{NH_4^+}$. In Fig. 6(b), the $E_{NH_4^+}$ for pH control 9.2 was the lowest, i.e., 12.5 MJ·kgN^{-1}, while the highest $E_{NH_4^+}$ was observed during pH control 10.5, i.e., 35.3 MJ·kgN^{-1}. In Fig. 6(a), the lowest $E_{NH_4^+}$ was observed at 40 A·m^{-2}, with achieved pH 9.2. However, a pH of 9.2 resulted in a poor stripping performance, due to the less converted NH_3 in the base and lower concentrations. The results indicate that CC application led to a greater increase in $E_{NH_4^+}$ compared to pH control. Eventually, the occurrence of scaling was less impactful for the experiments with pH control.

Previous studies showed similar energy requirements between 10.1 and 14.2 MJ·kgN^{-1}, as reported by (Rodrigues et al., 2021, 2020), when combining ED with Donnan Dialysis and trans-membrane chemisorption. (Ferrari et al., 2022) reported an energy consumption ranging from 23.7 to 47.8 MJ·kgN^{-1} in a pilot-scale BPMC with trans-membrane chemisorption, operated with "ON" and "OFF" cycles of applied current to achieve Donnan dialysis. However, in these studies a substantial

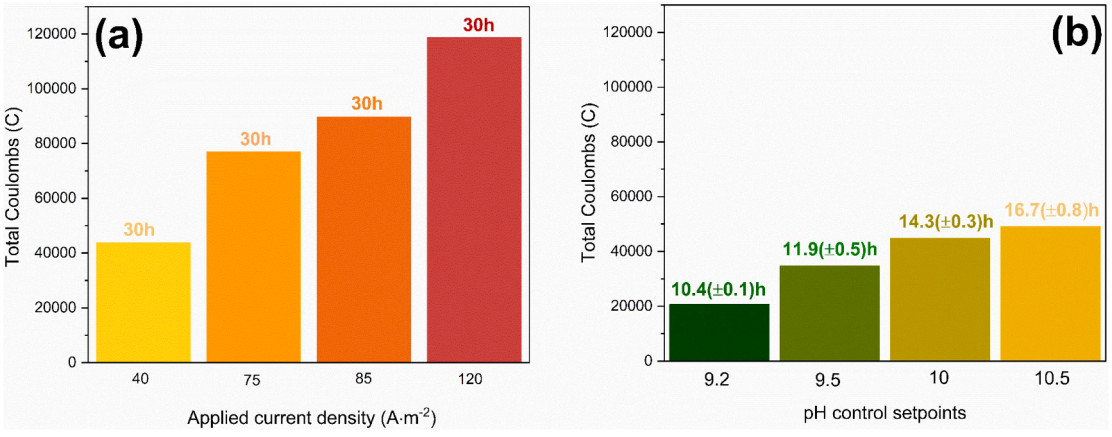

Fig. 5. The total coulombs (C) by the BPMC per targeted pH. (a) Total applied coulombs by BPMC after 30 h of operation under constant current. (b) Total coulombs by BPMC during 30 h of operation under pH control. The graph represents the summed coulombs for the indicated time in hours (h) that the PSU was ON.

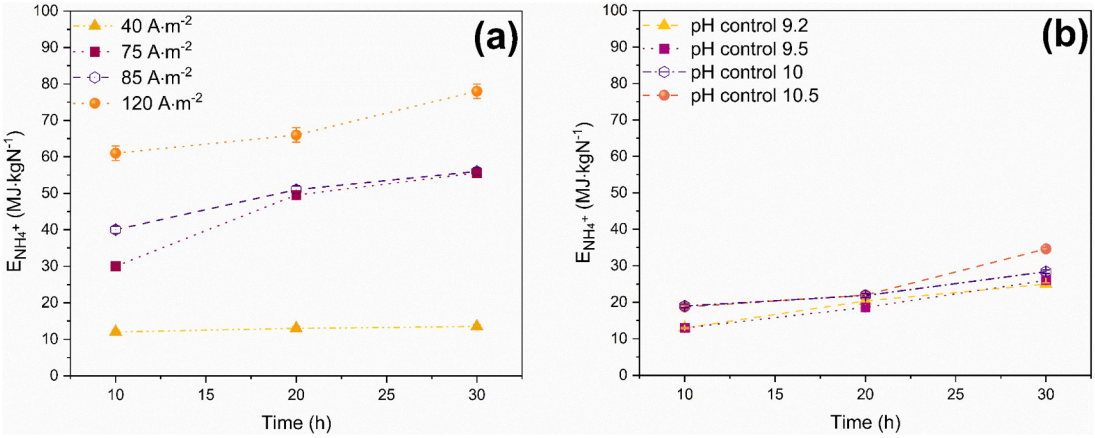

Fig. 6. The calculated $E_{NH_4^+}$ of BPMC for every 10 h. (a) The $E_{NH_4^+}$ during the CC operation under an I_d of 40, 75, 85, 120 A·m^{-2}. (b) The $E_{NH_4^+}$ during pH control operation for the targeted pH setpoints of 9.2, 9.5, 10 and 10.5.

decline in basicity is reported, with significant pH reduction occurring within 10 h of operation. In contrast, the present study demonstrates that a pH of 10 to 10.5 could be stably maintained for at least 30 h during the treatment of real reject water, without the need for external NaOH addition. As highlighted by van Linden et al. (2020b), the chemical energy demand associated with NaOH dosing in electrodialysis processes can account for even 50 % of the total energy input in ED. Therefore, the implementation of an internal pH control, offers a promising pathway to reduce operational costs.

3.4. NH_4^+ removal efficiency ($RE(t,\%)$) in BPMC under pH control and constant current (CC) operation

Fig. 7 shows the NH_4^+ removal efficiency ($RE(t,\%)$) for every experiment with pH control and CC method. The $RE(t,\%)$ of the BPMC is dependant to the I_d, operational method and expressed by the total transported mass of NH_4^+.

In Fig. 7(a), the $RE(t,\%)$ was improved for lower I_d. However, according to Ferrari et al. (2022) and Rodrigues et al. (2023), increasing the I_d in a BPMC configuration should lead to an improved $RE(t,\%)$. A key distinction in current study is that the BPMC was continuously fed by the SEDR providing NH_4^+ concentration in the acid which were at least a factor eight times higher than in the AD reject water of the feed. Consequently, the concentration of cations competing with NH_4^+ in the acid solution also increased. This suggests that higher I_d may have led to a reduced distribution of charge allocated to NH_4^+ transport, as previously shown in Fig. 4. Higher I_d led to higher basicity converting more NH_4^+ to NH_3 which could have resulted to more NH_3 back diffusion (van Linden et al., 2020b). In Fig. 7(b) The same reduction profile was also observed for the pH control method where the $RE(t,\%)$ is depicted in a declining trajectory per higher pH setpoint.

Additionally, a decreasing trend in $RE(t,\%)$ over time was observed for both methods, likely due to scaling formation on the CEM surface. Ion precipitation on the active pore sites of the membrane likely restricted pathways for NH_4^+ transport. Rodrigues et al. (2020) reported a similar decline in $RE(t,\%)$ over time in BPMC, attributing it to scaling formation on the CEM. The removal of NH_4^+ might be less favoured at the applied high I_d as described by the theoretical model of Rodrigues et al. (2021).

Nevertheless, despite the less applied coulombs during pH control, the $RE(t,\%)$ was comparable to the operation with CC and decreased over time similarly to CC. The $RE(t,\%)$ during pH control depended on the duration and frequency of the occurred pulses. During higher pH setpoints the duration of the pulses was longer with shorter frequency. Pulses of longer duration could have resulted to more transported competitive cations such as K^+, Ca^{2+} and Mg^{2+} combined with more CP occurrence. As a result, the $RE(t,\%)$ of pH control 10.5 was the lowest, ranging from 73 % to 67 %, while the highest efficiency was observed at a setpoint 9.2, ranging from 93 % to 90 %. Furthermore, the $RE(t,\%)$ during the first 10 h under pH control exceeded the $RE(t,\%)$ under the CC method for pH setpoints of 9.2, 9.5 and 10.

The mass of recovered NH_3 in the permeate increased with both higher I_d under CC operation and elevated pH setpoints under pH-controlled conditions. However, at higher pH levels, the increased

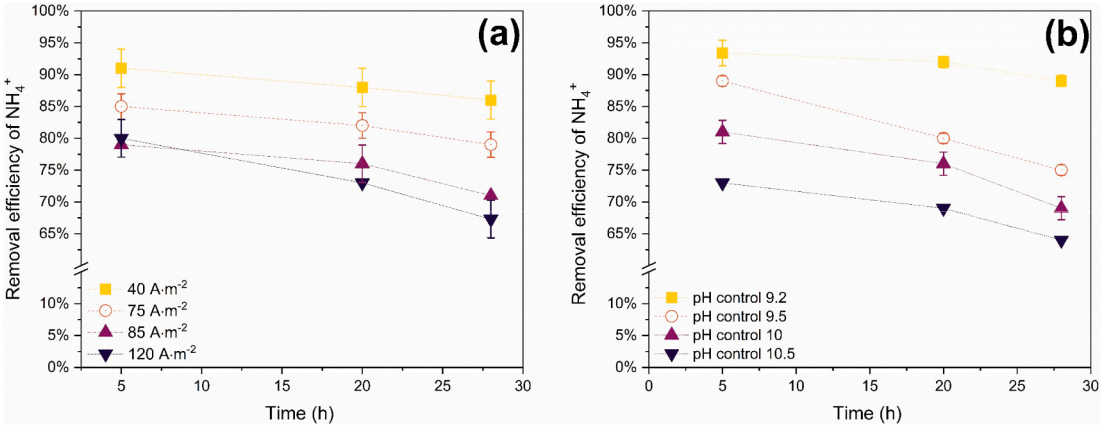

Fig. 7. The $RE(t,\%)$ in BPMC per hour for both operational methods. (a) The $RE(t,\%)$ under the CC method was calculated based on three sampling points. The experiments of 40, 75, 85 and 120 A·m^{-2} are represented. (b) The $RE(t,\%)$ with the pH control method for the targeted setpoints of pH 9.2, 9.5, 10 and 10.5.

volatility of NH_3 led to greater losses via evaporation through the vacuum pump. Additionally, enhanced back-diffusion of NH_3 was observed at elevated pH in the base solution, further diminishing the, $RE(t, \%)$. Despite the lower NH_3 concentrations observed in the permeate under pH control, this method resulted in a higher NH_3:H_2O purity ratio compared to the CC method (Table S1). This improvement in product purity is attributed to the reduced co-transport of competing cations during pulse-modulated current.

3.5. Total transported mass of NH_4^+ in the base solution

Fig. 8 shows the mass of NH_4^+ transported by BPMC for both operational procedures. Although, the applied pH control resulted in lower $E_{NH_4^+}$ and similar $RE(t, \%)$ with CC, yet the transported mass was lower compared to the CC method. Despite that diffusion provided an additional driving force for NH_4^+ transport under pH control, electromigration remained the dominant mechanism. Fig. 8(a) shows that the total transported mass with CC method, increased from 17 g to 27 g from 40 to 120 A m^{-2}, respectively. In Fig. 8(b), the total transported mass of NH_4^+ increased from an average of 7.1 to 22.3 for setpoints from 9.2 to 10.5, respectively. As a result, NH_4^+ mass transport was ultimately higher with the CC method. Similarly, Ferrari et al. (2022) showed that interrupted applied electric current results in less transported NH_4^+ compared to the constant current application. The pH control led to interrupted applied current, reducing the electrostatic force for ion transport (Fig. S2). Therefore, the recovered mass in the base was lower with pH control. Additionally, during the pH-control experiment, the final concentration in the base was slightly higher at a higher setpoint due to more applied coulombs at higher setpoints of pH.

In general, the application of pH control led to lower recovery of NH_4^+ in the base for every experiment. During pH control less transport of cations as Ca^{2+}, Mg^{2+} and CO_2 diffusion occurred in combination with restrained transport of total mass of NH_4^+ too.

While the pH-controlled BPMC configuration transported approximately 22–31 % less NH_4^+ compared to the CC operation, pH control achieved over 40 % reduction in total $E_{NH_4^+}$. The use of CC in BPMC for NH_3 recovery from real reject water led to earlier onset of membrane scaling, which in turn caused a decrease in local basicity and an increase in energy demand due to elevated membrane resistance, as also reported by Rodrigues et al. (2021), Saabas et al. (2024), and Ferrari et al. (2022).

Moreover, pH-controlled operation could reduce the need for frequent CIP cycles and external chemical consumption, ultimately decreasing operational expenditures and the cost per unit of removed ammonia. According to Ferrari et al. (2022) often CIP cycles degrade the membrane conductivity and structure. Therefore, less frequent CIP could also extend membrane lifespan. To mitigate scaling, partial removal of divalent cations (e.g., Ca^{2+} and Mg^{2+}) via nanofiltration softening can be considered as a viable pre-treatment (Zhou et al., 2023). Additionally, the combination of MCEMs with pulsed current modulation could further reduce the pre-treatment burden and associated costs, especially in scenarios where partial ion removal can be cost-effective than complete softening.

3.6. Future outlook

The principle of pH control in BPMED/BPMC/ED systems, facilitates flexible operations, especially when on-site conditions demand this. When recovery of NH_4^+ in the form of NH_3 is required for extraction via VMS, pH control offers an alternative approach to external NaOH dosing. Moreover, the marginal raises in $E_{NH_4^+}$ for increased pH-controlled setpoints offer potentials for higher basicity in the base. In future continuous operation at large scale, the developed pH control method can potentially reduce the operational costs. Furthermore, a hybrid approach combining CC and pH control can be applied strategically, depending on the primary objective: achieving higher concentration levels or reducing energy costs, respectively. Furthermore, pH control in the acid compartment can be investigated as future objective to minimize H_3O^+competition and CO_2 formation. This can be achieved by optimizing the load ratio in the SEDR unit, like pH control by feeding rate as demonstrated by Rodrigues et al. (2023). Moreover, CO_2 capture via CO_2-stripping could be implemented in the acid solution as an alternative for product generation (Sharifian et al. 2022). In applications aiming for NH_3 conversion, pH control in BPMC could offer the opportunity to reduce the external chemical addition of caustics without affecting the purity of the product.

4. Conclusions

Precise pH control is particularly critical for controlled NH_3 stripping in a two-compartment bipolar membrane electrodialysis (BPMC) system coupled with a vacuum membrane stripping (VMS) unit. The results demonstrated that implementing pH control allowed in-situ control of the pH in the base solution within the BPMC. Thus, making it feasible within an SEDR+BPMC+VMS configuration to consistently direct the level of desired basicity for NH_3 conversion during stripping. The pH control method led to a more favourable distribution of the electric current toward NH_4^+ transport, improving the current efficiency ($\eta_{\%}$) and positively impacting the energy consumption ($E_{NH_4^+}$). The developed pH control method minimised electric current usage, while the targeted pH setpoint was maintained. Although the removal efficiencies ($RE(t,$

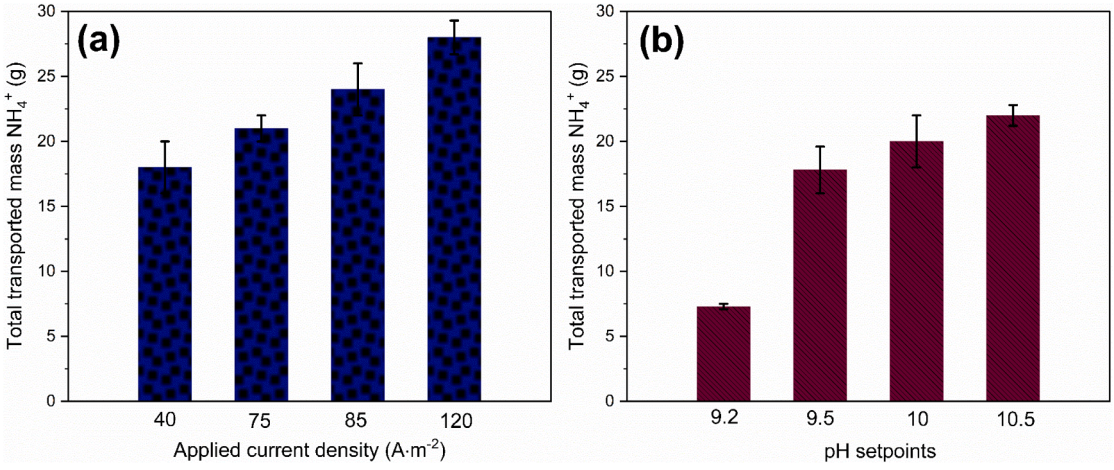

Fig. 8. Total transported mass of NH_4^+ by the BPMC. (a) CC method at current densities of 40, 75, 85 and 120 (A·m^{-2}). (b) pH control method at pH setpoints 9.2, 9.5, 10 and 10.5.

%)) for both methods were similar at comparable setpoints, pH control notably minimized scaling formation, as indicated by the lower $E_{NH_4^+}$ compared to the continuous current (CC) method. However, pH control resulted in a lower recovered mass of NH_4^+ compared to CC, likely due to less applied coulombs and activation time of the power supply unit. Specifically, the following conclusions can be drawn:

- The BPMC maintained a similar $\eta_{\%}$ across all pH setpoints (25–29 %) under pH control, while $\eta_{\%}$ for the CC method declined from 28 % to 12 % for higher current densities.
- The $RE(t, \%)$ under pH control ranged from 66 % to a maximum of 94 %, although both methods exhibited a decreasing in $RE(t, \%)$ over time, likely due to scaling formation.
- At pH setpoints of 9.5, 10, and 10.5, $E_{NH_4^+}$ with pH control remained between 15 and 35 MJ·kgN^{-1}, whereas $E_{NH_4^+}$ for the CC method started at 30 MJ·kgN^{-1} and increased to 76 MJ·kgN^{-1}.
- In future applications, the pH control method could be further utilised in BPMED/BPMC systems for the recovery of CO_2 and NH_3 by precisely controlling their pKa and pKb values, thereby reducing the required electrical energy input and external chemical dosing.

CRediT authorship contribution statement

Iosif Kaniadakis: Writing – original draft, Methodology, Investigation, Data curation, Conceptualization. **Jules B. van Lier:** Validation, Supervision, Resources, Project administration, Funding acquisition. **Henri Spanjers:** Validation, Supervision, Investigation, Formal analysis.

Declaration of competing interest

The authors declare the following financial interests/personal relationships which may be considered as potential competing interests: Iosif Kaniadakis reports financial support was provided by Delft University of Technology. Iosif Kaniadakis reports a relationship with Delft University of Technology that includes: employment. Iosif Kaniadakis has patent pending to Delft University of Technology. If there are other authors, they declare that they have no known competing financial interests or personal relationships that could have appeared to influence the work reported in this paper.

Acknowledgements

This work was financially supported by the Netherlands Enterprise Agency, also known as Rijksdienst voor Ondernemend Nederland (RVO), through the Demonstration of Energy Innovation (DEI+) grant CEI120070. Additionally, the research received a contribution from the Foundation for Applied Water Research (STOWA). The authors would like to acknowledge the valuable contributions of the following project partners: Blue-Tec BV, W&F Technologies BV, i3 Innovative Technologies BV, Waterschapsbedrijf Limburg, Waterschap Amstel, Gooi en Vecht. The authors would like to thank Sam Molenaar for his valuable contribution to technical supervision.

Supplementary materials

Supplementary material associated with this article can be found, in the online version, at doi:10.1016/j.watres.2025.124185.

Data availability

Data will be made available on request.

References

Andreeva, M.A., Gil, V.V., Pismenskaya, N.D., Dammak, L., Kononenko, N.A., Larchet, C., Grande, D., Nikonenko, V.V., 2018. Mitigation of membrane scaling in electrodialysis by electroconvection enhancement, pH adjustment and pulsed electric field application. J. Membr. Sci. 549, 129–140. https://doi.org/10.1016/J.MEMSCI.2017.12.005.

Arslan, D., Zhang, Y., Steinbusch, K.J.J., Diels, L., Hamelers, H.V.M., Buisman, C.J.N., De Wever, H., 2017. In-situ carboxylate recovery and simultaneous pH control with tailor-configured bipolar membrane electrodialysis during continuous mixed culture fermentation. Sep. Purif. Technol. 175, 27–35. https://doi.org/10.1016/j.seppur.2016.11.032.

Blommaert, M.A., Aili, D., Tufa, R.A., Li, Q., Smith, W.A., Vermaas, D.A., 2021. Insights and challenges for applying bipolar membranes in advanced electrochemical energy systems. ACS Energy Lett. 6 (7), 2539–2548. https://doi.org/10.1021/acsenergylett.1c00618.

Capdevila-Cortada, M., 2019. Electrifying the haber–bosch. Nature Catal. 2 (12), 1055. https://doi.org/10.1038/s41929-019-0414-4.

Chen, Y., Edwards, B.L., Dasgupta, P.K., Srinivasan, K., 2012. pH- and Concentration-Programmable electrodialytic buffer generator. Anal. Chem. 84 (1), 59–66. https://doi.org/10.1021/ac2023734.

Deng, Z., van Linden, N., Guillen, E., Spanjers, H., van Lier, J.B., 2021. Recovery and applications of ammoniacal nitrogen from nitrogen-loaded residual streams: a review. J. Environ. Manage. 295, 113096. https://doi.org/10.1016/J.JENVMAN.2021.113096.

EL-Bourawi, M.S., Khayet, M., Ma, R., Ding, Z., Li, Z., Zhang, X., 2007. Application of vacuum membrane distillation for ammonia removal. J. Membr. Sci. 301 (1–2), 200–209. https://doi.org/10.1016/j.memsci.2007.06.021.

Ferrari, F., Pijuan, M., Molenaar, S., Duinslaeger, N., Sleutels, T., Kuntke, P., Radjenovic, J., 2022. Ammonia recovery from anaerobic digester centrate using onsite pilot scale bipolar membrane electrodialysis coupled to membrane stripping. Water Res. 218, 118504. https://doi.org/10.1016/J.WATRES.2022.118504.

Guillen-Burrieza, E., Moritz, E., Hobisch, M., Muster-Slawitsch, B., 2023. Recovery of ammonia from centrate water in urban waste water treatment plants via direct contact membrane distillation: process performance in long-term pilot-scale operation. J. Membr. Sci. 667, 121161. https://doi.org/10.1016/J.MEMSCI.2022.121161.

Guo, X., Chen, J., Wang, X., Li, Y., Liu, Y., Jiang, B., 2023. Sustainable ammonia recovery from low strength wastewater by the integrated ion exchange and bipolar membrane electrodialysis with membrane contactor system. Sep. Purif. Technol. 305, 122429. https://doi.org/10.1016/j.seppur.2022.122429.

Honarparvar, S., Al-Rashed, R., Winter, V., A.G., 2023. Investigation of pulsed electric field operation as a chemical-free anti-scaling approach for electrodialysis desalination of brackish water. Desalination 551, 116386. https://doi.org/10.1016/j.desal.2023.116386.

Ippersiel, D., Mondor, M., Lamarche, F., Tremblay, F., Dubreuil, J., Masse, L., 2012. Nitrogen potential recovery and concentration of ammonia from swine manure using electrodialysis coupled with air stripping. J. Environ. Manage. 95 (SUPPL), S165–S169. https://doi.org/10.1016/J.JENVMAN.2011.05.026.

Jiang, C., Zhang, Y., Feng, H., Wang, Q., Wang, Y., Xu, T., 2017. Simultaneous CO2 capture and amino acid production using bipolar membrane electrodialysis (BMED). J. Membr. Sci. 542, 264–271. https://doi.org/10.1016/j.memsci.2017.08.004.

Kamcev, J., Paul, D.R., Manning, G.S., Freeman, B.D., 2018. Ion diffusion coefficients in ion exchange membranes: significance of counterion condensation. Macromolecules 51 (15), 5519–5529. https://doi.org/10.1021/acs.macromol.8b00645.

Kaniadakis, I., van Lier, J.B., Spanjers, H., 2024. Removal of total ammoniacal nitrogen from reject water through selective electrodialysis reversal and bipolar electrodialysis. Chem. Eng. J. 493, 152613. https://doi.org/10.1016/j.cej.2024.152613.

Kattan Readi, O.M., Kuenen, H.J., Zwijnenberg, H.J., Nijmeijer, K., 2013. Novel membrane concept for internal pH control in electrodialysis of amino acids using a segmented bipolar membrane (sBPM). J. Membr. Sci. 443, 219–226. https://doi.org/10.1016/j.memsci.2013.04.045.

Kotoka, F., Gutierrez, L., Verliefde, A., Cornelissen, E., 2024. Selective separation of nutrients and volatile fatty acids from food wastes using electrodialysis and membrane contactor for resource valorization. J. Environ. Manage. 354, 120290. https://doi.org/10.1016/j.jenvman.2024.120290.

Kyriakou, V., Garagounis, I., Vourros, A., Vasileiou, E., Stoukides, M., 2020. An electrochemical haber-bosch process. Joule 4 (1), 142–158. https://doi.org/10.1016/j.joule.2019.10.006.

Li, Y., Shi, S., Cao, H., Wu, X., Zhao, Z., Wang, L., 2016. Bipolar membrane electrodialysis for generation of hydrochloric acid and ammonia from simulated ammonium chloride wastewater. Water Res. 89. https://doi.org/10.1016/j.watres.2015.11.038.

Li, Y., Wang, R., Shi, S., Cao, H., Yip, N.Y., Lin, S., 2021. Bipolar membrane electrodialysis for ammonia recovery from synthetic urine: experiments, modeling, and performance analysis. Environ. Sci. Technol. 55 (21), 14886–14896. https://doi.org/10.1021/acs.est.1c05316.

Limoli, A., Langone, M., Andreottola, G., 2016. Ammonia removal from raw manure digestate by means of a turbulent mixing stripping process. J. Environ. Manage. 176, 1–10. https://doi.org/10.1016/J.JENVMAN.2016.03.007.

Mani, K.N., 1991. Electrodialysis water splitting technology. J. Membr. Sci. 58 (2), 117–138. https://doi.org/10.1016/S0376-7388(00)82450-3.

Mohammadi, M., Guo, H., Yuan, P., Pavlovic, V., Barber, J., Kim, Y., 2021. Ammonia separation from wastewater using bipolar membrane electrodialysis. Electrochem. Sci. Adv. 1 (4). https://doi.org/10.1002/elsa.202000030.

Mondor, M., Masse, L., Ippersiel, D., Lamarche, F., Massé, D.I., 2008. Use of electrodialysis and reverse osmosis for the recovery and concentration of ammonia from swine manure. Bioresour. Technol. 99 (15), 7363–7368. https://doi.org/10.1016/J.BIORTECH.2006.12.039.

Mutahi, G., van Lier, J.B., Spanjers, H., 2024. Leveraging organic acids in bipolar membrane electrodialysis (BPMED) can enhance ammonia recovery from scrubber effluents. Water Res. 265, 122296. https://doi.org/10.1016/j.watres.2024.122296.

Nomura, Y., Iwahara, M., Hongo, M., 1988. Acetic acid production by an electrodialysis fermentation method with a computerized control system. Appl. Environ. Microbiol. 54 (1), 137–142. https://doi.org/10.1128/aem.54.1.137-142.1988.

Ozkul, S., Arbabzadeh, O., Bisselink, R.J.M., Kuipers, N.J.M., Bruning, H., Rijnaarts, H.H.M., Dykstra, J.E., 2024. Selective adsorption in ion exchange membranes: the effect of solution ion composition on ion partitioning. Water Res. 254, 121382. https://doi.org/10.1016/j.watres.2024.121382.

Ozkul, S., van Daal, J.J., Kuipers, N.J.M., Bisselink, R.J.M., Bruning, H., Dykstra, J.E., Rijnaarts, H.H.M., 2023. Transport mechanisms in electrodialysis: the effect on selective ion transport in multi-ionic solutions. J. Membr. Sci. 665, 121114. https://doi.org/10.1016/j.memsci.2022.121114.

Palakodeti, A., Rupani, P.F., Azman, S., Dewil, R., Appels, L., 2022. Novel approach to ammonia recovery from anaerobic digestion via side-stream stripping at multiple pH levels. Bioresour. Technol. 361, 127685. https://doi.org/10.1016/J.BIORTECH.2022.127685.

Pärnamäe, R., Mareev, S., Nikonenko, V., Melnikov, S., Sheldeshov, N., Zabolotskii, V., Hamelers, H.V.M., Tedesco, M., 2021. Bipolar membranes: a review on principles, latest developments, and applications. J. Membr. Sci. 617, 118538. https://doi.org/10.1016/J.MEMSCI.2020.118538.

Paul, D.R., 2004. Reformulation of the solution-diffusion theory of reverse osmosis. J. Membr. Sci. 241 (2), 371–386. https://doi.org/10.1016/J.MEMSCI.2004.05.026.

Quist-Jensen, C.A., Wybrandt, L., Løkkegaard, H., Antonsen, S.B., Jensen, H.C., Nielsen, A.H., Christensen, M.L., 2018. Acidification and recovery of phosphorus from digested and non-digested sludge. Water Res. 146, 307–317. https://doi.org/10.1016/J.WATRES.2018.09.035.

Rathod, N.H., Upadhyay, P., Sharma, V., Kulshrestha, V., 2024. Designing and development of stable asymmetric bipolar membrane for improved water splitting and product recovery by electrodialysis. J. Membr. Sci. 695, 122427. https://doi.org/10.1016/j.memsci.2024.122427.

Rodrigues, M., Molenaar, S., Barbosa, J., Sleutels, T., Hamelers, H.V.M., Buisman, C.J.N., Kuntke, P., 2023. Effluent pH correlates with electrochemical nitrogen recovery efficiency at pilot scale operation. Sep. Purif. Technol. 306, 122602. https://doi.org/10.1016/J.SEPPUR.2022.122602.

Rodrigues, M., Paradkar, A., Sleutels, T., Heijne, A.ter, Buisman, C.J.N., Hamelers, H.V.M., Kuntke, P., 2021. Donnan dialysis for scaling mitigation during electrochemical ammonium recovery from complex wastewater. Water Res. 201, 117260. https://doi.org/10.1016/j.watres.2021.117260.

Rodrigues, M., Sleutels, T., Kuntke, P., Hoekstra, D., ter Heijne, A., Buisman, C.J.N., Hamelers, H.V.M., 2020. Exploiting donnan dialysis to enhance ammonia recovery in an electrochemical system. Chem. Eng. J. 395, 125143. https://doi.org/10.1016/j.cej.2020.125143.

Rodríguez Arredondo, M., Kuntke, P., ter Heijne, A., Hamelers, H.V.M., Buisman, C.J.N, 2017. Load ratio determines the ammonia recovery and energy input of an electrochemical system. Water Res. 111, 330–337. https://doi.org/10.1016/J.WATRES.2016.12.051.

Saabas, D., Lee, J., 2022. Recovery of ammonia from simulated membrane contactor effluent using bipolar membrane electrodialysis. J. Membr. Sci. 644, 120081. https://doi.org/10.1016/J.MEMSCI.2021.120081.

Sharifian, R., Blommaert, M.A., Bremer, M., Wagterveld, R.M., Vermaas, D.A., 2021. Intrinsic bipolar membrane characteristics dominate the effects of flow orientation and external pH-profile on the membrane voltage. J. Membr. Sci. 638, 119686. https://doi.org/10.1016/j.memsci.2021.119686.

Sharifian, R., Boer, L., Wagterveld, R.M., Vermaas, D.A., 2022. Oceanic carbon capture through electrochemically induced in situ carbonate mineralization using bipolar membrane. Chem. Eng. J. 438, 135326. https://doi.org/10.1016/j.cej.2022.135326.

Shi, L., Hu, Y., Xie, S., Wu, G., Hu, Z., Zhan, X., 2018. Recovery of nutrients and volatile fatty acids from pig manure hydrolysate using two-stage bipolar membrane electrodialysis. Chem. Eng. J. 334, 134–142. https://doi.org/10.1016/j.cej.2017.10.010.

Sosa-Fernandez, P.A., Post, J.W., Ramdlan, M.S., Leermakers, F.A.M., Bruning, H., Rijnaarts, H.H.M., 2020. Improving the performance of polymer-flooding produced water electrodialysis through the application of pulsed electric field. Desalination 484, 114424. https://doi.org/10.1016/j.desal.2020.114424.

Strathmann, H., 2010. Electrodialysis, a mature technology with a multitude of new applications. Desalination 264 (3), 268–288. https://doi.org/10.1016/J.DESAL.2010.04.069.

Sun, B., Zhang, M., Huang, S., Cao, Z., Lu, L., Zhang, X., 2022. Study on mass transfer performance and membrane resistance in concentration of high salinity solutions by electrodialysis. Sep. Purif. Technol. 281, 119907. https://doi.org/10.1016/j.seppur.2021.119907.

Tanaka, Y., 2007. Chapter 7 Donnan dialysis. Membr. Sci. Technol. 12, 495–503. https://doi.org/10.1016/S0927-5193(07)12021-0.

Tran, A.T.K., Jullok, N., Meesschaert, B., Pinoy, L., Van der Bruggen, B., 2013. Pellet reactor pretreatment: a feasible method to reduce scaling in bipolar membrane electrodialysis. J. Colloid Interface Sci. 401, 107–115. https://doi.org/10.1016/j.jcis.2013.03.036.

Valluri, S., Kawatra, S.K., 2021. Reduced reagent regeneration energy for CO2 capture with bipolar membrane electrodialysis. Fuel Process. Technol. 213, 106691. https://doi.org/10.1016/j.fuproc.2020.106691.

van Linden, N., Bandinu, G.L., Vermaas, D.A., Spanjers, H., van Lier, J.B., 2020b. Bipolar membrane electrodialysis for energetically competitive ammonium removal and dissolved ammonia production. J. Cleaner Prod. 259, 120788. https://doi.org/10.1016/J.JCLEPRO.2020.120788.

van Linden, N., Spanjers, H., van Lier, J.B., 2019. Application of dynamic current density for increased concentration factors and reduced energy consumption for concentrating ammonium by electrodialysis. Water Res. 163, 114856. https://doi.org/10.1016/j.watres.2019.114856.

van Linden, N., Spanjers, H., van Lier, J.B., 2022. Fuelling a solid oxide fuel cell with ammonia recovered from water by vacuum membrane stripping. Chem. Eng. J. 428, 131081. https://doi.org/10.1016/j.cej.2021.131081.

van Linden, N., Wang, Y., Sudhölter, E., Spanjers, H., van Lier, J.B., 2022. Selectivity of vacuum ammonia stripping using porous gas-permeable and dense pervaporation membranes under various hydraulic conditions and feed water compositions. J. Membr. Sci. 642, 120005. https://doi.org/10.1016/J.MEMSCI.2021.120005.

Ward, A.J., Arola, K., Thompson Brewster, E., Mehta, C.M., Batstone, D.J., 2018. Nutrient recovery from wastewater through pilot scale electrodialysis. Water Res. 135, 57–65. https://doi.org/10.1016/J.WATRES.2018.02.021.

Wijmans, J.G., Baker, R.W., 1995. The solution-diffusion model: a review. J. Membr. Sci. 107 (1–2), 1–21. https://doi.org/10.1016/0376-7388(95)00102-I.

Wu, J., Jiang, Z., Xie, H., Fan, J., Lou, Y., Liu, J., Chen, S., Liu, Y., Ye, X., 2025. An innovative pH control strategy for alleviating membrane fouling in bipolar membrane electrodialysis during ultraviolet stabilizer production wastewater treatment. Sep. Purif. Technol. 362, 131749. https://doi.org/10.1016/j.seppur.2025.131749.

Yang, D., Liu, H., She, Q., 2023. Mixed cation transport behaviours in electrodialysis during simultaneous ammonium enrichment and wastewater desalination. Desalination 545, 116155. https://doi.org/10.1016/j.desal.2022.116155.

Zhou, Z., Zhang, M., Xia, Q., Zhao, X., Ming, Q., Zeng, L., 2023. Effects of nanofiltration on desalination of flue gas desulfurization wastewater by electrodialysis: treatment effect, fouling property and techno-economic analysis. Sep. Purif. Technol. 316, 123768. https://doi.org/10.1016/j.seppur.2023.123768.